Effects of morphology on mechanical properties of a SBS triblock copolymer

I. Yamaoka* and M. Kimura
Advanced Materials and Technology Research Laboratories, Nippon Steel Corporation, 1618 Ida, Nakahara-ku, Kawasaki 211, Japan
(Received 3 June 1992; revised 20 January 1993)

The morphology and mechanical properties of the mouldings of a poly(styrene-*block*-butadiene-*block*-styrene) triblock copolymer (KR05, Phillips Petroleum Co.) were examined. All the mouldings exhibit lamellar morphology and their mechanical properties depended on the lamellar orientation. KR05 with oriented lamellae shows excellent Izod impact strength and large elongation since under tensile stress the lamellae shear yield extensively with dominant expansion and cavitation of the polybutadiene lamellae. That with wavy lamellae shows enhanced rigidity and heat resistance since the lamellae also shear yield but offer more resistance against the deformation because of the close and complicated networks of the polybutadiene phase with the rigid polystyrene phase. Stereoscopic structural examination of the mouldings revealed that the appreciable mechanical anisotropy results from the anisotropy of the microdomain structure formed on cooling the melt.

(Keywords: block copolymer; mechanical properties: morphology)

INTRODUCTION

Among the alloying techniques of polymers investigated and made practical, block copolymerization is classified as a very important approach for modifying the properties of the component polymers. Since the length of the component blocks and the existence of chemical linkages between immiscible blocks limit the phase separation in block copolymers, microdomain structure with a finer dispersion of the various phases can be obtained. One of the most representative examples is the styrene–butadiene block copolymer, which has attracted considerable attention both from the scientific and the technological points of view[1–8]. The polybutadiene (PB) and polystyrene (PS) blocks in the block copolymer develop typical morphologies in which the two components segregate into separate phases present in a spherical, rod-like or lamellar form on the scale of hundreds or thousands of ångström[5], and consequently bring a unique combination of rubbery and plastic properties.

Although the principal microdeformation process in many styrene-based polymers is crazing[2,9], the mode of microdeformation induced in the styrene–butadiene block copolymer depends strongly on the morphology and the microdomain orientation. For example, crazing was the main fracture mechanism of some styrene–butadiene block copolymers of spherical[2,7] or cylindrical PB domain morphology[8], while crazing and shear yielding were observed for the lamellae which were oriented parallel to the stretching direction and for those which were oriented randomly, respectively[10]. Only a few reports have dealt with the bulky products of styrene–butadiene block copolymer of great industrial use, such as injection mouldings and compression mouldings[10], although the microdomain structure of the copolymer films has been widely characterized[1,2,4,7,8]. In this paper, therefore, a commercial styrene–butadiene block copolymer was injection- and compression-moulded and the effects of the morphology on the mechanical properties of the mouldings were investigated.

* To whom correspondence should be addressed

EXPERIMENTAL

Materials

A commercial star-shaped poly(styrene-*block*-butadiene-*block*-styrene) triblock copolymer (SBS) manufactured by the Phillips Petroleum Company under the trade name of K-Resin KR05 was used. A star-shaped block copolymer was chosen because it has the advantage of greater stiffness over the linear block copolymers of equivalent styrene–butadiene composition and block molecular weights[11]. The number- and weight-average molecular weights (M_n and M_w) and the ratio M_w/M_n for KR05 used were 5.23×10^4, 1.51×10^5 and 2.69, respectively, shown using g.p.c. N.m.r. measurements revealed that KR05 had a 0.245 weight fraction of a PB block component. Measurements by d.s.c. showed two distinct glass transition temperatures (T_gs) near -80 and 95°C corresponding to the PB and PS phases, respectively.

Sample preparation

KR05 was melt processed in two ways, namely, by injection moulding and by compression moulding.

Injection moulding. As-received pellets of KR05 were injection-moulded with a Toshiba IS100E injection moulding machine into impact, tensile and flexural test bars with the corresponding thicknesses of 6.35 mm

0032-3861/93/214399-11

(0.25 in.), 3.2 mm (0.125 in.) and 6.35 mm (0.25 in.), respectively. The flexural bars were also used to measure the deflection temperature under flexural load. The barrel temperature, mould temperature and injection rate were set at 210°C, 40°C and 40 $cm^3 s^{-1}$, respectively.

Compression moulding. (1) 'Rapidly-cooled KR05'. As-received pellets of KR05 were compression-moulded at 200°C for 5 min into three types of rectangular plaques of different thickness (150 × 150 × 3.0 mm, 4.0 mm and 6.0 mm), followed by cooling the hot moulds rapidly. Cooling was carried out by running cold water through pipes in the mould clamping plates of the pressing machine so that the mould temperature dropped to 50°C in 3 min. Subsequently, these plaques were machined with metal templates into impact (4.0 mm thick), tensile (3.0 mm) and flexural (6.0 mm) test bars, respectively. The flexural bars were also used to measure the deflection temperature. All test bars were cut out at inner regions far from the sides of these plaques, because the end effect of microdomain structure on mechanical properties could be ignored, that is, the disturbance of microdomain structure due to melt flow complexity near the plaque sides during compression moulding could be ignored.

(2) 'Slowly-cooled KR05'. Impact test bars (4.0 mm thick) were machined from inner regions of KR05 plaques (150 × 150 × 4.0 mm), which were compression-moulded at 200°C for 5 min followed by cooling very slowly by controlling the temperature of the pressing machine with the mould kept on compression between the mould clamping plates. The mould temperature dropped to ~50°C in 6 h.

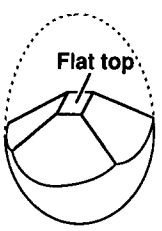

Figure 1 Diagram showing a pyramid-shaped piece cut from the as-received KR05 pellet. A flat top on the piece was made for later microtoming

Mechanical tests

The notched Izod impact strength was measured at 23°C according to ASTM D256 using a pendulum type tester. Tensile and three-point loading flexural tests were carried out on a conventional Instron testing machine at 23°C according to ASTM D638 and ASTM D790, respectively. The deflection temperature under flexural load was measured under the maximum fibre stress of 1820 kPa according to ASTM D648.

Examination of microdomain structure

Morphologies of as-received pellets of KR05 and their mouldings were observed with transmission electron microscopy (TEM). The oval-shaped pellets were machined into pyramid-shaped pieces, as shown in *Figure 1*. Their apexes were cut off for later microtoming. Similar pyramid-shaped pieces were cut out of inner regions of injection-moulded impact test bars and of compression-moulded plaques (4.0 mm thick), as shown in *Figure 2*. In the case of injection-moulded bars the *Y* axis was fixed parallel to the melt flow direction during injection moulding. In the case of compression-moulded plaques the axes of coordinates were fixed so that the *X* direction was identical to the compressive direction and the *XZ* plane was parallel to the operating side and also the backside of the pressing machine. Apexes of the pyramid-shaped pieces from the mouldings were cut off to expose the surfaces of the plane of interest (*XY*, *XZ* or *YZ* plane) on the resultant flat tops of the pieces. After treatment with a 2% aqueous solution of osmium tetroxide, ultra-thin sections (500–900 Å thick) were cut from the flat tops of the pieces using a LKB microtome with a diamond knife. Sections were observed by using a Hitachi H700 transmission electron microscope at an accelerating voltage of 100 kV, and routine magnifications of 30 000 × and 100 000 × were used.

The following method was used to examine the deformation of microdomain structure in the injection-moulded KR05 and the compression-moulded KR05 ('rapidly-cooled KR05') after tensile stress application. Tensile bars were pulled at 50 mm min^{-1} up to break on an Instron testing machine. Then pyramid-shaped pieces with flat tops as described in *Figure 2* were cut out of the regions close to fracture surfaces so that the

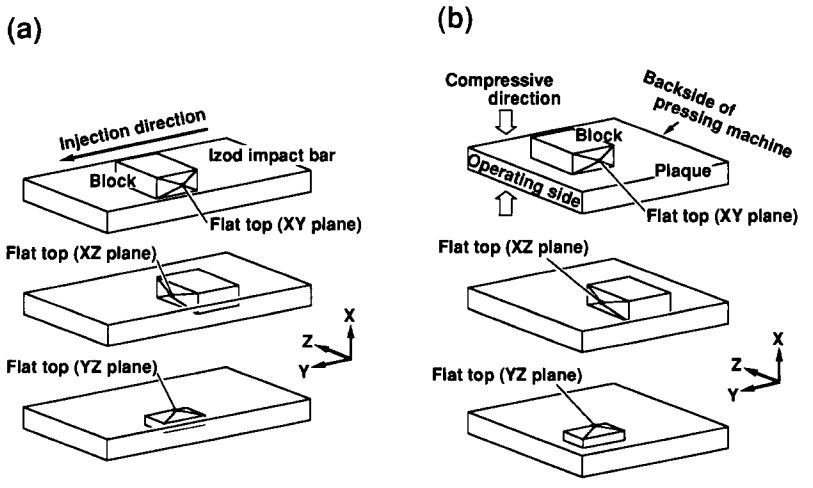

Figure 2 Diagram showing pyramid-shaped pieces cut from (a) injection-moulded and (b) compression-moulded plaques. Note that the *Y* and the *X* axes are fixed in the injection direction for (a) and the compressive direction for (b), respectively. Flat tops on pieces were made for microtoming parallel to the *XY*, *XZ* or *YZ* plane

morphological changes of KR05 on fracture could be observed. After sufficient staining and hardening of the PB phase of KR05 in a 2% aqueous solution of osmium tetroxide to reduce additional deformation during microtoming[12], ultra-thin sections were microtomed parallel to the tensile direction on flat tops of the pieces with a diamond knife. Several days were needed to sufficiently harden the surface regions of the pieces as at room temperature osmium tetroxide diffused slowly from the outer surfaces to a depth of a few micrometres.

RESULTS AND DISCUSSION

Microdomain structure and fracture mechanism

Figure 3 shows transmission electron micrographs of the as-received KR05. The morphology was viewed at the inner region of a pellet (*Figure 1*). *Figure 3b* is a higher magnification view of *Figure 3a*. KR05 exhibited a lamellar type phase separation, in which the stained dark PB phase and the bright PS phase formed alternating lamellae with thicknesses of 150–200 and 200–250 Å, respectively. *Figure 3* revealed that the lamellar morphology was incomplete since many parts of the PB lamellae were disconnected in the PS matrix phase. The lamellae were randomly oriented, which suggested that KR05 could not be subjected to a large anisotropic stress in the pelletizing process.

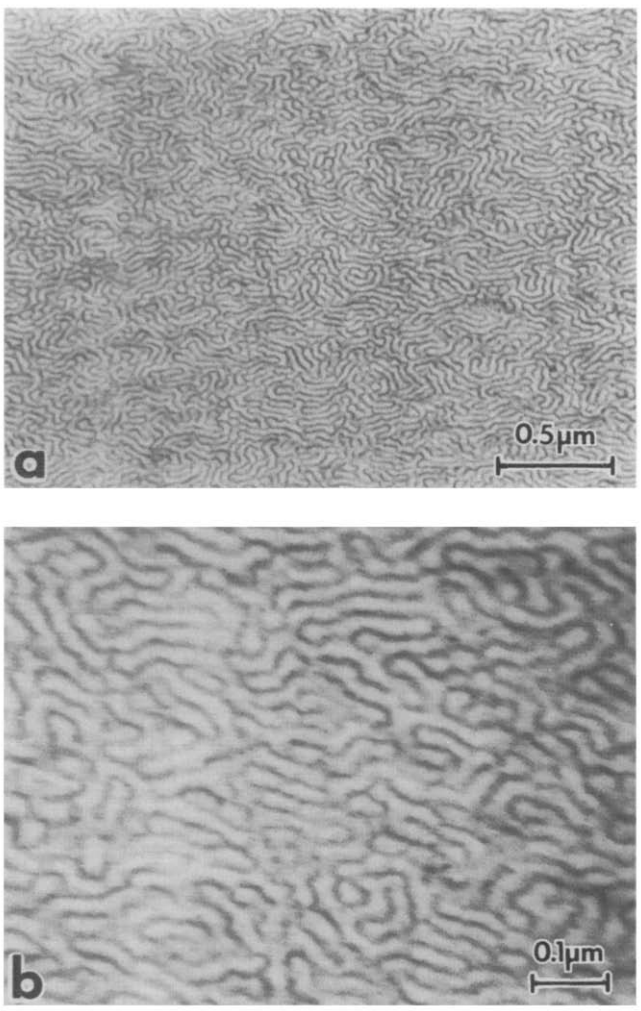

Figure 3 Transmission electron micrographs of as-received KR05. (b) is a higher magnification view of (a)

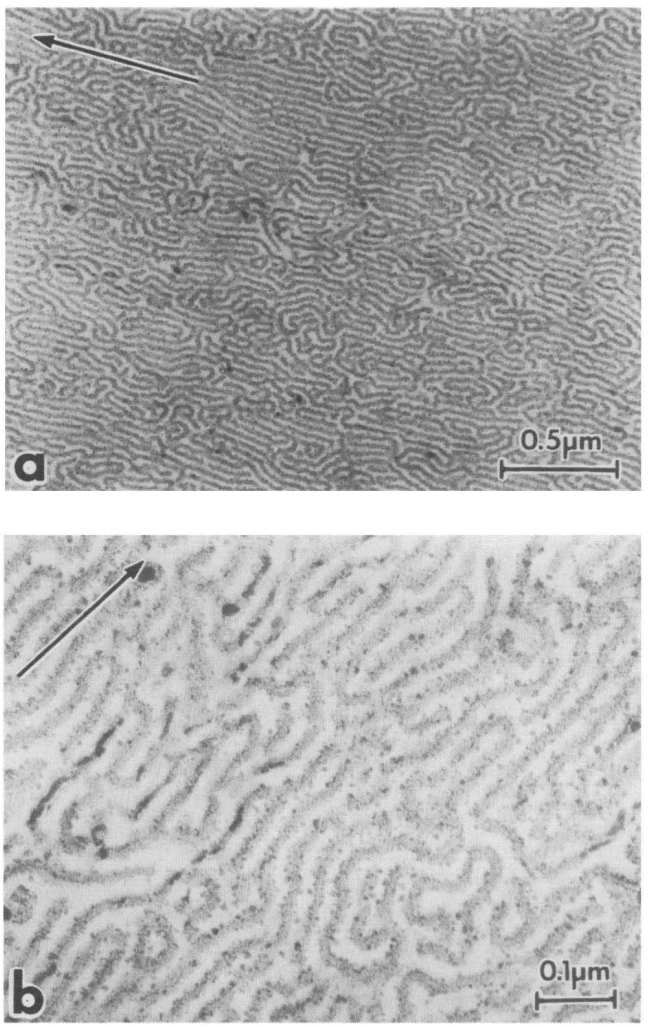

Figure 4 Transmission electron micrographs of injection-moulded KR05. The morphology was viewed on the *XY* plane (see *Figure 2a*). (b) is a higher magnification view of (a). The arrows show the injection directions

Figure 4 shows transmission electron micrographs of the injection-moulded KR05. The morphology was viewed on the *XY* plane at the core region of an Izod impact test bar (*Figure 2a*). *Figure 4b* is a higher magnification view of *Figure 4a*. The injection-moulded KR05 exhibited an incomplete lamellar morphology in which many parts of the PB lamellae were disconnected in the PS matrix phase, similar to the morphology of the as-received KR05. The lamellae were wavy and almost randomly oriented, but seemed to be oriented in the injection direction (shown by arrows on the micrographs) despite the morphology observed on sections from the core region of the injection mouldings. This suggests that lamellar orientation, which might be induced by shear flow behind the melt front on mould filling[13], could not be totally relaxed because the melt viscosity increased very rapidly as the resin temperature fell in the cold mould.

Figure 5a shows the stress–strain behaviour of the injection-moulded KR05 specimen up to the point of break. It was found to be similar to that of the other SBS of alternating lamellar morphology with 52 wt% PB reported previously[14–16], except for the large difference in elongation at break between the former (~50%) and the latter (~370%). After the KR05 specimen went

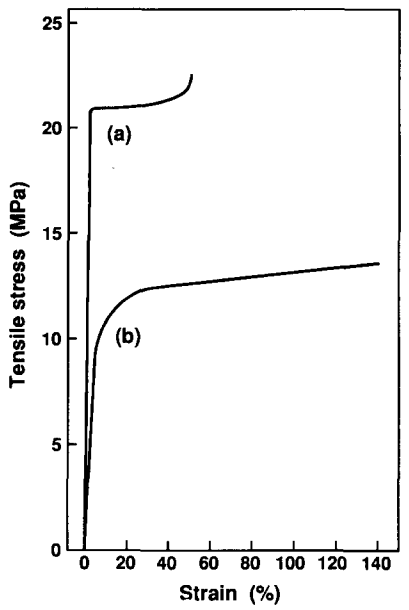

Figure 5 Tensile stress–strain behaviour of (a) injection-moulded KR05 and (b) 'rapidly-cooled KR05' at room temperature at a constant strain rate of 50 mm min^{-1}

through a yield point on stretching, the stress remained constant for a moment and then increased gently until the whole specimen was thinned with apparent necking. The stress–strain curve sloped more steeply with increasing strain. Further stretching resulted in a sharp stress increase soon followed by fracture.

The injection-moulded KR05 did not exhibit a high degree of strain recovery even after several months following release from tension before fracture, while the SBS with 52 wt% PB exhibited prominent strain recovery from a large extension in a few days[14–16]. This might be due to the difference in the styrene–butadiene composition between the two SBSs.

Figure 6 shows the deformation structure observed in the region close to the fracture surface after tensile stress application to the injection-moulded specimen of KR05. *Figure 6b* is a higher magnification view of *Figure 6a*. Comparison between the morphologies of an unstretched (*Figure 4*) and a stretched (*Figure 6*) specimen revealed considerable structural change on stretching in the direction shown by the arrows on *Figure 6* at 50 mm min^{-1} up to the point of break. Randomly oriented lamellae of an unstretched specimen (*Figure 4*) were deformed irregularly by predominant shear yielding to oriented and destructive lamellae of a stretched one (*Figure 6*). In more detail, the PS lamellae surrounding the intermittent PB lamellae in an unstretched state (*Figure 4*) were fragmented as the strain increased, and the consequent gradual phase inversion finally resulted in separate PS domains dispersed in the PB lamellae. Since all broken specimens examined showed the same structural changes as in *Figure 6*, macroscopic plastic deformation of the injection-moulded KR05 occurred through such extensive shear yielding. If the deformation process on stretching for randomly oriented lamellae of the injection-moulded KR05 was similar to that proposed previously for the randomly oriented lamellae of SBS[14–16], the deformation structure as in *Figure 6* must have resulted through shearing, kinking, destruction and reorientation of the KR05 lamellae accompanied by fragmentation of the PS major phase. The fragmentation of lamellar microdomains presumably developed after the yielding point[15], and could be accelerated when a sharp stress increase occurred on the stress–strain curve after the whole specimen completed thinning (see *Figure 5a*).

It is strongly suggested by previous studies[10,14–16] that shear yielding should be dominant in the lamellae which are randomly oriented or oriented perpendicular to the stretching direction, while crazing should occur in the lamellae oriented in the stretching direction. However, it should be noted that the opposite result was observed in the study[6] where the tensile fracture mechanism of KR03 sheets, which is also a SBS in the K-Resin family but another grade to the KR05 used here, was examined. KR03 and KR05 are chemically equivalent and the only difference between the two is the gel content of the resin[17]. Although the KR03 lamellae were oriented perpendicular to the stretching direction, crazing prevailed on fracture[6].

Figure 7 shows transmission electron micrographs of the compression-moulded KR05, which was obtained by cooling hot moulds rapidly, designated 'rapidly-cooled KR05'. The morphology was viewed on the *XZ* plane at the core region of a 4 mm thick plaque. A higher

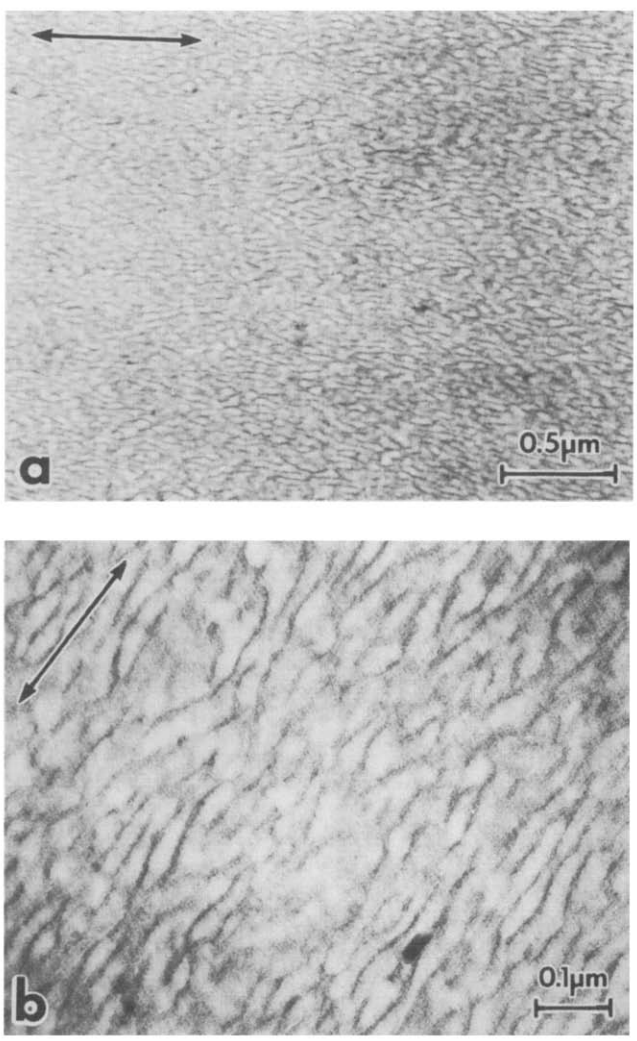

Figure 6 Transmission electron micrographs of injection-moulded KR05 fractured under tensile stress. Morphological change was observed on longitudinal cross-sections just below the fracture surface. (b) is a higher magnification view of (a). The arrows show the tensile directions

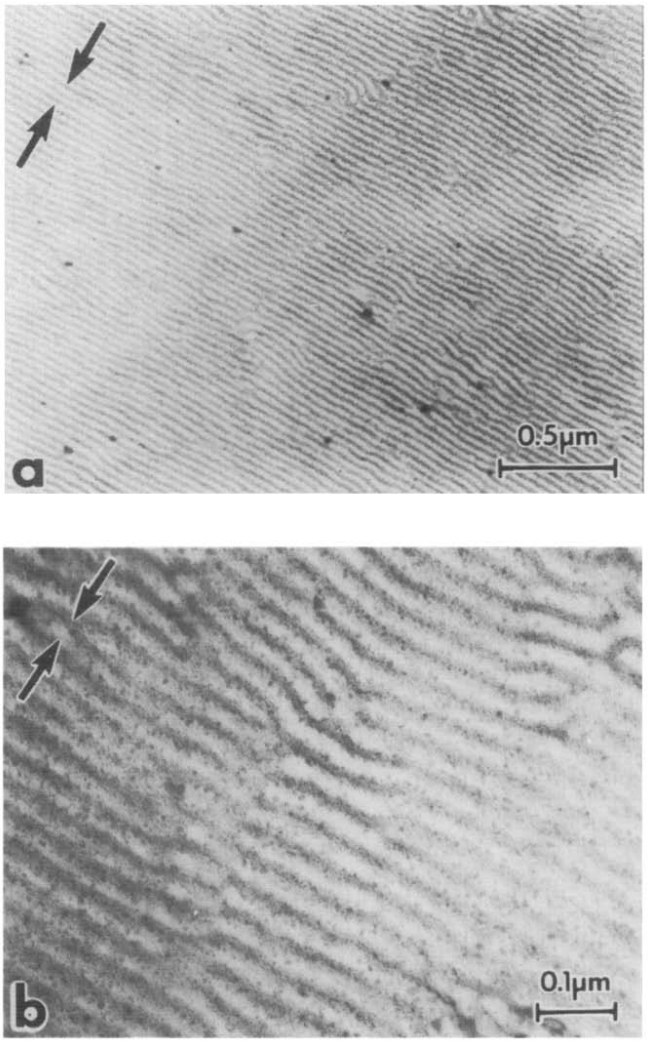

Figure 7 Transmission electron micrographs of compression-moulded KR05 designated 'rapidly-cooled KR05'. The morphology was viewed on the *XZ* plane (see *Figure 2b*). (b) is a higher magnification view of (a). The arrows show the compressive directions

magnification view of *Figure 7a* is shown in *Figure 7b*. The arrows on the micrographs show the *X* direction (i.e. compressive direction). The compression-moulded KR05 also exhibited lamellar type morphology, in which the stained PB phase and the bright PS phase formed alternating lamellae with thicknesses of 150–200 and 200–250 Å, respectively. Lamellae were not corrugated and formed orderly layers unlike the wavy lamellae of the as-received and the injection-moulded KR05 (*Figures 3* and *4*). However, long range order in the lamellae of 'rapidly-cooled KR05' was not as perfect as that for a layered structure of plywood. There was a kind of line defect (dislocation) in some places, where the extra PB lamella emanated from the side of the PB lamella. These defects were responsible for the PS lamellae being disconnected in places.

Figure 5b shows the typical stress–strain behaviour of 'rapidly-cooled KR05' specimens, which was somewhat different from that of the injection-moulded samples (*Figure 5a*). The former did not exhibit a clear yielding point although a gradual transition from elastic to plastic deformation was observed. After the elastic deformation of the KR05 specimen was completed, the slope of the stress–strain curve became gentler as strain increased, and then remained constant until the whole specimen was thinned without apparent necking, followed by fracture. Larger elongation at break (110–140%) than that for the injection-mouldings (~50%) was observed. 'Rapidly-cooled KR05' did not exhibit such high strain recovery from an extension as the SBS with 52 wt% PB[14–16], which could be due to the high styrene content of KR05.

Figure 8 shows the deformation structure observed in the region close to the fracture surface after the application of tensile stress to the 'rapidly-cooled KR05' specimen. Comparison between the morphologies of an unstretched (*Figure 7a*) and a stretched (*Figure 8*) specimen revealed considerable structural change on stretching in the direction shown by the arrows on *Figure 8* up to the point of break. Oriented lamellae of an unstretched specimen were deformed regularly in zigzags by predominant shear yielding. The PS lamellae were not fragmented and the continuity of the lamellae was kept even in the region close to the fracture surface. Since all broken specimens examined showed the same structural changes as in *Figure 8*, macroscopic plastic deformation of 'rapidly-cooled KR05' occurred through extensive shear band development.

The black dots seen on the micrograph (*Figure 8*) suggest that an early stage of cavitational breakdown in the PB phase resulted in preferential fixing by subsequent osmium tetroxide treatment[6]. These microcavities were responsible for whitening (opacity) in the region near the fracture surface. After sufficient yielding development, final fracture must have resulted from the growth of microcavities to local microcracks and further macrocrack propagation.

As can be seen in *Figure 5*, the injection-moulded KR05 showed larger tensile stress (i.e. larger resistance to deformation) on stretching than 'rapidly-cooled KR05'. This could result from the close and complicated networks of the PB lamellae with the rigid PS lamellae formed in the injection-moulded KR05 (*Figure 4*). Lamellar orderliness of 'rapidly-cooled KR05' could allow one-sided expansion of the soft PB phase on stretching because the morphology showed no networks effective to avoid the large deformation of the PB phase (*Figure 7*). The rapid and excessive stretching of

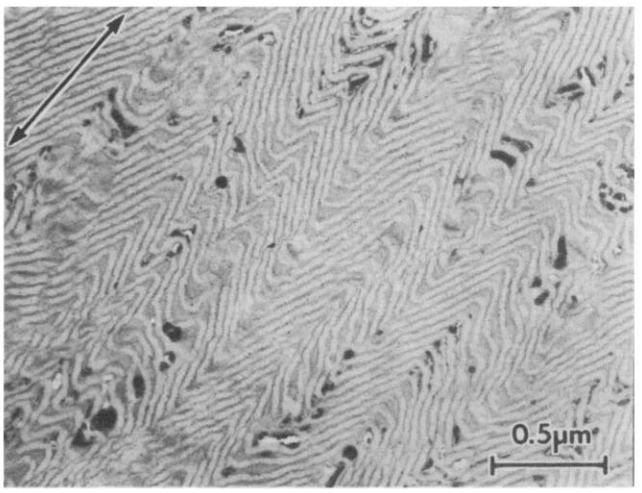

Figure 8 Transmission electron micrograph of 'rapidly-cooled KR05' fractured under tensile stress. Morphological change was observed on a longitudinal cross-section just below the fracture surface. The arrow shows the tensile direction

'rapidly-cooled KR05' must have induced the large dilational stress, which resulted in the cavitation in the PB phase.

The expansion of lamellar spacing and the formation of zigzag-shaped lamellae of 'rapidly-cooled KR05' were the same phenomena as observed in the earlier stage of deformation proposed for the other SBS[14–16]. However, in the case of 'rapidly-cooled KR05' the synchronous deformation process was not fragmentation but cavitation. The reason is as yet unknown, but could be related to the high styrene content and the lack of necking in 'rapidly-cooled KR05' on stretching.

Mechanical properties

Table 1 summarizes the mechanical properties of the injection-moulded KR05 and the 'rapidly-cooled KR05'. There were significant differences in the mechanical properties between the two mouldings. The mechanical properties of the KR05 mouldings depended on the lamellar orientation relative to the stretching direction. 'Rapidly-cooled KR05' of orderly oriented lamellae showed much greater impact strength and larger elongation at break than the injection-moulded KR05 of randomly oriented lamellae, whereas the latter was superior to the former in strength, modulus and deflection temperature under flexural load. This suggests that for KR05, orderly oriented lamellae should be more effective for enhancing toughness than randomly oriented ones, and vice versa for rigidity and heat resistance.

On stretching of 'rapidly-cooled KR05', the PB lamellae were expanded more than the PS lamellae up to the point of break as discussed above. In this case, the large deformation of the PB rubber could be responsible for the better toughness but lead to inferior rigidity because the dilational stress might act mainly in the soft PB phase. However, the injection-moulded KR05 did not show large expansion but offered large resistance to plastic deformation of the PB lamellae, which must have resulted from the close and complicated networks of the PB lamellae with the rigid PS lamellae, leading to superior rigidity.

Table 1 Mechanical properties of injection-moulded KR05 and compression mouldings designated 'rapidly-cooled KR05'

Moulding method	Injection moulding	Compression moulding	
Machine direction		*Y*	*Z*
Izod impact strength ($J\,m^{-1}$)	19.6	77.5 (*Zi*)[a]	229 (*Yi*)[b]
Tensile strength (MPa)	22.6	14.6	13.6
Tensile modulus (MPa)	1230	728	534
Elongation at break (%)	50	110	140
Flexural strength (MPa)	33.3	12.6	12.1
Flexural modulus (MPa)	1470	661	535
Deflection temperature under flexural load (°C) (Fibre stress 1820 kPa)	71	57	56

[a] Striking direction *Zi*
[b] Striking direction *Yi*

Anisotropy of microdomain structure

'Rapidly-cooled KR05' showed noticeable mechanical anisotropy with the mechanical properties varying depending on the direction in which test bars were machined off, as shown in *Table 1*. It is of interest that similar appreciable mechanical anisotropy was previously found for extruded specimens of SBS[1,5]. The stereoscopic microdomain structure of 'rapidly-cooled KR05' was examined since the mechanical anisotropy was expected to result from the anisotropy of the microdomain structure caused by the definite lamellar orientation in KR05. *Figure 9* shows transmission electron micrographs of 'rapidly-cooled KR05', taken on *XY*, *XZ* and *YZ* planes at the core region of a 4 mm thick plaque as described in *Figure 2*. The arrows on the micrographs show the *X* direction in which the material was compressed. *Figure 9* suggests that the stereoscopic anisotropy of the microdomain structure existed in 'rapidly-cooled KR05' since lamellae viewed on the *XZ* and *YZ* planes were regularly oriented in definite directions whereas those as viewed on the *XY* plane were wavy.

Several 'rapidly-cooled KR05' mouldings were examined by TEM to model the stereoscopic microdomain structure. Ultra-thin sections were carefully microtomed

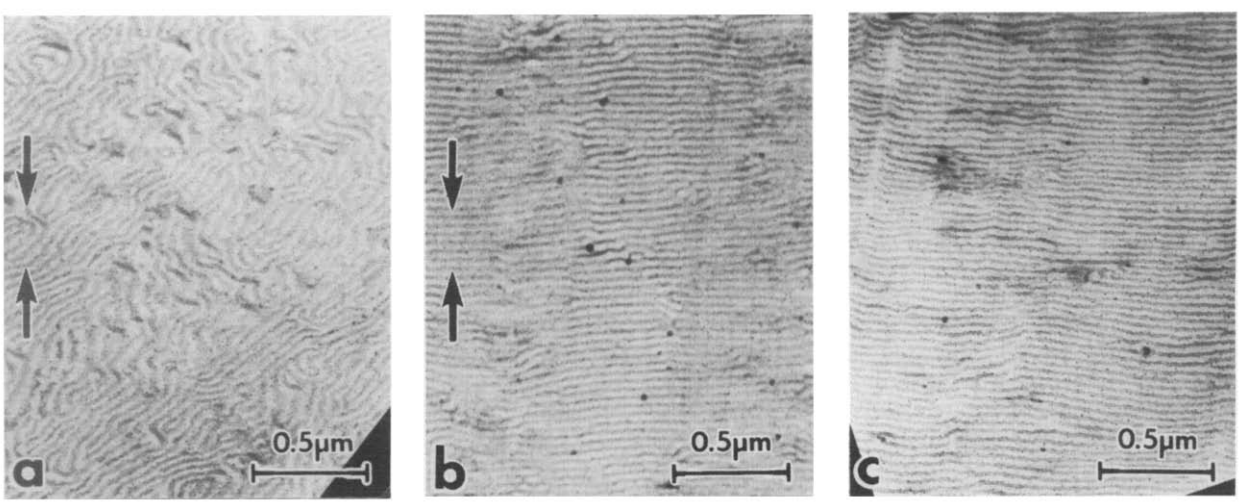

Figure 9 Transmission electron micrographs of 'rapidly-cooled KR05'. The morphology was observed on the three different planes which meet at right angles as described in *Figure 2b*: (a) *XY* plane; (b) *XZ* plane; (c) *YZ* plane. The arrows show the compressive directions

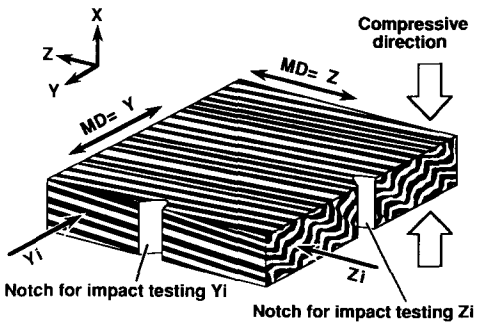

Striking direction	Yi	Zi
Izod impact strength (J/m)	229	77.5

Figure 10 Speculative model of stereoscopic microdomain structure of a 'rapidly-cooled KR05' plaque. Note that lamellar thickness is greatly exaggerated for the plaque dimensions. Arrows *Yi* and *Zi* exhibit the pendulum-striking directions for impact test bars machined in the *Z* and *Y* directions, respectively. The table shows the notched Izod impact strength of the test bars

as exactly on the *XY* plane in the *Y* direction as possible so that microscratches produced by a knife edge could become references to examine the direction of the lamellar orientation. Similarly, the other ultra-thin sections were microtomed exactly on the *XZ* plane in the *X* direction, or on the *YZ* plane in the *Y* direction. The directions of the lamellar orientation relative to the *X*, *Y* or *Z* direction were examined by tracing microscratches seen on the micrographs in order to model stereoscopic arrangements of KR05 lamellae. *Figure 10* represents a speculative model of the stereoscopic microdomain structure of 'rapidly-cooled KR05' plaques. This model reflects the stereoscopic microdomain structure of all the test bars very well, since they were cut out from the inner regions where end effects, as mentioned earlier, could be ignored. In this model, the lamellar thickness of the plaque is exaggerated so that the lamellar arrangements can be clearly seen. The lamellae, as viewed on the *XZ* and the *YZ* planes, were regularly oriented with some angle to the *Z* direction, and therefore alternating layers of the PB and the PS phases stratified obliquely to the plaque surface (i.e. the *YZ* plane). However, the lamellae as viewed on the *XY* plane were wavy and less aligned similar to those observed in the injection-moulded KR05 (*Figure 4*). Such anisotropic microdomain structure was reproduced as long as the same cooling rate as for the hot moulds was adopted on compression moulding.

The partial anisotropy of the microdomain structure which appeared in the 'rapidly-cooled KR05' plaques could be due to the following reason. It was previously observed that interfaces between the PS and the polydiene phases of some styrene–diene block copolymers with lamellar or cylindrical phase separations were oriented parallel to the surfaces of cast films[18–20] or extrudates[5]. These phenomena should be due to gradual one-by-one phase separation or interface rearrangement of sytrene–diene block copolymers which began at surface regions of the bulk and proceeded in the thickness direction, since the direction of solvent transfer in cast films or heat transfer in extrudates was roughly perpendicular to their surfaces. During conventional compression moulding, heat conducts mainly through the thickness of the mouldings in a pseudo-stationary state on cooling. However, in the 'rapidly-cooled KR05' plaques studied here, the direction of the main heat transfer could not be normal to the plaque surfaces (i.e. the *YZ* plane) and varied with time even at the core regions of the plaques. This is because cooling was not carried out uniformly due to the unbalanced layout of the water-cooling pipes which were embedded in the mould clamping plates of the pressing machine. This was probably the factor most responsible for the partial anisotropy of the microdomain structure in the 'rapidly-cooled KR05' plaques as modelled in *Figure 10*, as the interface rearrangement of the KR05 from the plaque surface to the core region could occur in the changeable direction of heat transfer.

Mechanical anisotropy

To examine the effects of the anisotropy of the microdomain structure of the 'rapidly-cooled KR05' plaques on the mechanical properties, test bars were machined from compression-moulded plaques in the *Y* and *Z* directions which meet each other at right angles. In the case of Izod impact testing the pendulum-striking direction was normal to the machine direction (MD) of the test bar. Arrows *Yi* and *Zi* in *Figure 10* show the pendulum-striking directions for impact test bars machined in the *Z* and *Y* directions, respectively. *Figures 11* and *12* show the pendulum-striking directions and the geometry of the impact test bars machined in the *Z* and *Y* directions, respectively. (a) and (b) in *Figures 11* and *12* show a front view and a side view of a test bar in a vice, respectively. In (b), the striking direction is normal to the figure.

In the case of tensile testing, the direction of tensile stress application was identical to the MD of the test bars as shown in *Figure 13*. In the cases of flexural testing and deflection temperature measurement, the direction of stress application was also identical to the MD of the test bars as shown in *Figure 14*. It should be noted that on three point loading compressive stress was induced at the upper skin regions in test bars on specimen supports, while tensile stress was induced at the lower

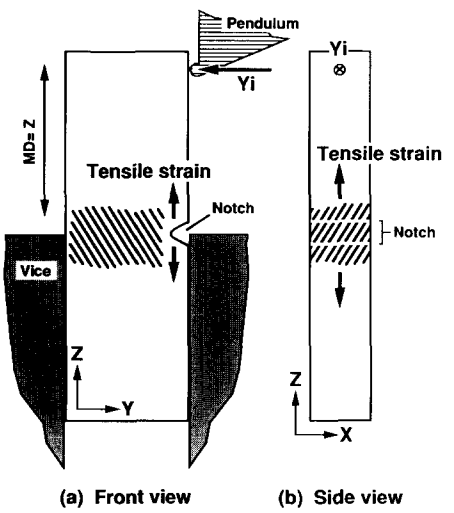

Figure 11 Schematic diagram of pendulum-striking to an Izod impact test bar of 'rapidly-cooled KR05' machined in the *Z* direction. The striking direction was *Yi*. (a) and (b) show a front view and a side view of a test bar in a vice, respectively. In (b), the striking direction *Yi* is shown normal to the figure. Images of KR05 lamellar arrangements on *YZ* and *XZ* planes subjected to tensile strain on impact are illustrated in (a) and (b), respectively

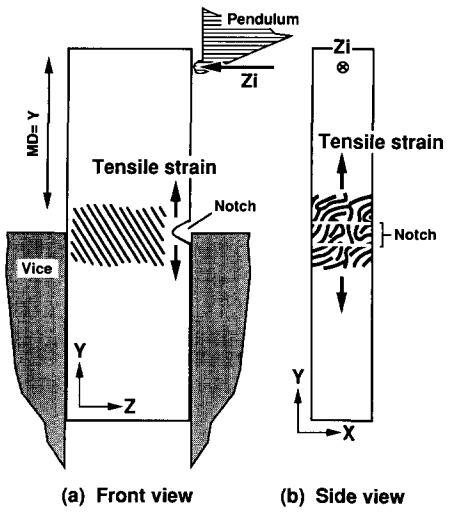

Figure 12 Schematic diagram of pendulum-striking to an Izod impact test bar of 'rapidly-cooled KR05' machined in the *Y* direction. The striking direction was *Zi*. (a) and (b) show a front view and a side view of a test bar in a vice, respectively. In (b), the striking direction *Zi* is shown normal to the figure. Images of KR05 lamellar arrangements on *YZ* and *XY* planes subjected to tensile strain on impact are illustrated in (a) and (b), respectively

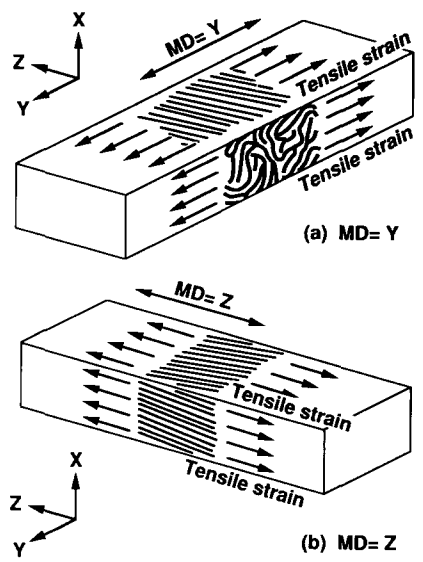

Figure 13 Schematic diagram of narrow sections of dumb-bell-shaped test bars of 'rapidly-cooled KR05' under tension. (a) and (b) show the bars machined in the *Y* and *Z* directions, respectively. The tensile direction was identical to the machine direction (MD). Images of KR05 lamellar arrangements on planes subjected to tensile strain are illustrated.

skin regions and interlayer shear stress at the core. In *Figures 11–14*, images of KR05 lamellar arrangements on the respective planes are illustrated with the lamellar thickness greatly exaggerated.

The mechanical properties are shown in *Table 1*. In the case of Izod impact data, a set of test bars machined in the *Z* direction (pendulum-struck in the *Yi* direction) showed higher impact strength than another set of bars machined in the *Y* direction (struck in the *Zi* direction). The difference in the deformation mechanism of the KR05 lamellae between the two sets may account for this phenomenon. Impact in the *Yi* direction gave rise to instantaneous tensile stress in the *Z* direction at the notch tip zone of the test bar (*Figure 11*). Such stress presumably caused zigzag-shaped deformation with large extension and cavitation of KR05 lamellae oriented orderly with some angle to the *MD* on both the *XZ* and *YZ* planes, and consequently a large amount of impact energy would be effectively dissipated. On the other hand, impact in the *Zi* direction gave rise to tensile stress in the *Y* direction at the notch tip zone of the test bar (*Figure 12*). Randomly oriented lamellae viewed on the *XY* plane could resist dilational stress because of their complicated networks. Consequently, impact energy absorption would not be very effective.

Anisotropic tensile and flexural properties are shown in *Table 1*. On these testings stresses were induced in the MDs of test bars as shown in *Figures 13* and *14*. Test bars machined in the *Y* direction could offer large resistance to plastic deformation since close and complicated networks of the lamellae were formed on the *XY* plane, which was one of the two planes where stress was induced on testing. On the other hand, test bars machined in the *Z* direction must have been more easily plastic-deformed because of orderly lamellae viewed on both the *XZ* and *YZ* planes where stress was induced on testing. This could result in the enhanced strength and modulus of the test bars cut out in the *Y* direction.

Order–disorder transition of KR05

Leibler[21] proposed that, at equilibrium, the parameters related to the phase separation of the AB-type diblock copolymer are given by the product χN (where χ is the A–B interaction parameter and N is the polymerization index) and f, the copolymer chain composition. When χN is larger than a certain value $(\chi N)_t$ for a given f, the copolymer exhibits phase separation. This theory has been found applicable to the ABA-type triblock copolymer[22] and the $(AB)_n$ star-shaped block copolymer (where n is the number of arms)[23]. As classically derived, the χ parameter of the block copolymer must decrease as a function of temperature, at least for fs for which phase separation occurs. This is, as a matter of course, the case with the styrene–diene block copolymer since observed

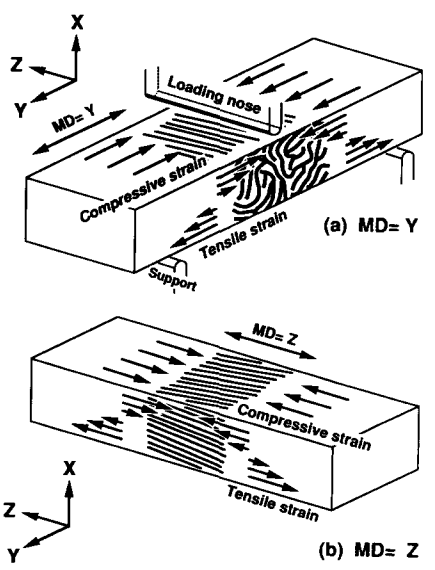

Figure 14 Schematic diagram of test bars of 'rapidly-cooled KR05' under three-point bending. (a) and (b) show the bars machined in the *Y* and *Z* directions, respectively. The direction of stress application was identical to the machine direction (MD). Images of KR05 lamellar arrangements on planes subjected to strain are illustrated

phase behaviour of the copolymer was of the upper critical solution temperature type[24,25]. In order to put the copolymer with larger N in a disordered state, the χ parameter must be smaller (i.e. temperature must be higher) so that χN of the copolymer may be smaller than $(\chi N)_t$. This implies that the transition temperature of the copolymer increases with an increase of molecular weight for a given f. This can be exemplified with two styrene–butadiene block copolymers with similar f, one with a viscosity-average molecular weight (M_v) of 70 000 and 71.4 wt% PB[22] and another with M_v of 57 000 and 74.6 wt% PB[26–29]. The former showed a transition temperature of 220°C, far higher than the value of 140–150°C for the latter. [Note that M_v is a little less than M_w for linear type molecules ($M_n < M_v \leqslant M_w$).]

The above discussion suggested that KR05 with a larger M_w of 151 000 should possess a very high transition temperature and exhibit phase separation in the ordered state at the resin temperature of 210°C on melt processing. In the moulding process, the memory of the lamellar morphology which was already formed in the as-received KR05, as shown in *Figure 3*, would not be initialized, and only the reorientation or lattice ordering of the lamellae could occur.

Effects of cooling rate

When the KR05 melt with lamellar type phase separation is cooled in the mould, the cooling rate of the melt should affect the lamellar orientation of the resultant plaques. During injection moulding of the KR05 in this study, the resin temperature dropped to ~50°C in 30 s after mould filling, which was the same as in conventional injection moulding. Materials filled into cold mould cavities on injection moulding were cooled much more rapidly than those on compression moulding adopted here. Therefore, on injection moulding, lamellae in the melt were solidified in the non-equilibrium state with an intensive shear field and a steep temperature gradient, in contrast to the case of the compression mouldings. *Figure 15* shows transmission electron micrographs of the injection-moulded KR05, taken on XY, XZ and YZ planes at the core region of Izod impact test bars (see *Figure 2a*). The micrographs show that all lamellae viewed on the XY, XZ and YZ planes of the injection mouldings are very wavy. This is due to cooling in the non-equilibrium state. The degree of overall lattice disorder of the lamellar arrangement in the injection-moulded KR05 was larger than that in 'rapidly-cooled KR05' since the former showed outstanding lamellar disorder on all the planes (*Figure 15*), whereas the latter showed appreciable lamellar disorder only on the XY plane (*Figures 9* and *10*). This suggests that lamellae of 'rapidly-cooled KR05' were more relaxed for the slower cooling rate.

There was no difference in the respective thicknesses of the PB and PS phases between the injection-moulded KR05 and 'rapidly-cooled KR05', in spite of the significant difference in the cooling rate between the two. This suggests that the interface between the PB and PS phases in the melt was well developed and stabilized, and lamellar thicknesses were hardly varied on cooling.

As 'rapidly-cooled KR05' was subject to solidification in a pseudo-stationary state with a temperature gradient kept gentle on cooling, all the lamellae viewed on the XY, XZ and YZ planes should be much more uniformly relaxed than the lamellae in injection mouldings. However, the partial anisotropy of the microdomain structure appeared in 'rapidly-cooled KR05', in which lamellae viewed on the XZ and YZ planes were well relaxed while those on the XY plane were still very wavy (*Figures 9* and *10*). This could arise from the unstable heat transfer on compression moulding as mentioned earlier. Attempts were made to cool the KR05 melt very slowly so that heat transfer could be greatly decelerated. *Figure 16* shows transmission electron micrographs of 'slowly-cooled KR05', taken on the XY, XZ and YZ planes at the core region of a 4 mm thick plaque. 'Slowly-cooled KR05' was subject to solidification with a temperature gradient kept very gentle on cooling, which could occur in an equilibrium state. Clear and orderly lamellae were seen on the XY and XZ planes but no lamellar structure was observed on the YZ plane. Since structural analyses of 'slowly-cooled KR05' plaques always led to the same results as seen in *Figure 16*, it is obvious that the lamellae were oriented roughly parallel to the plaque surfaces (i.e. the YZ plane) on slow cooling. The thicknesses of the PB and PS phases of 'slowly-cooled KR05' were the same as those for the injection

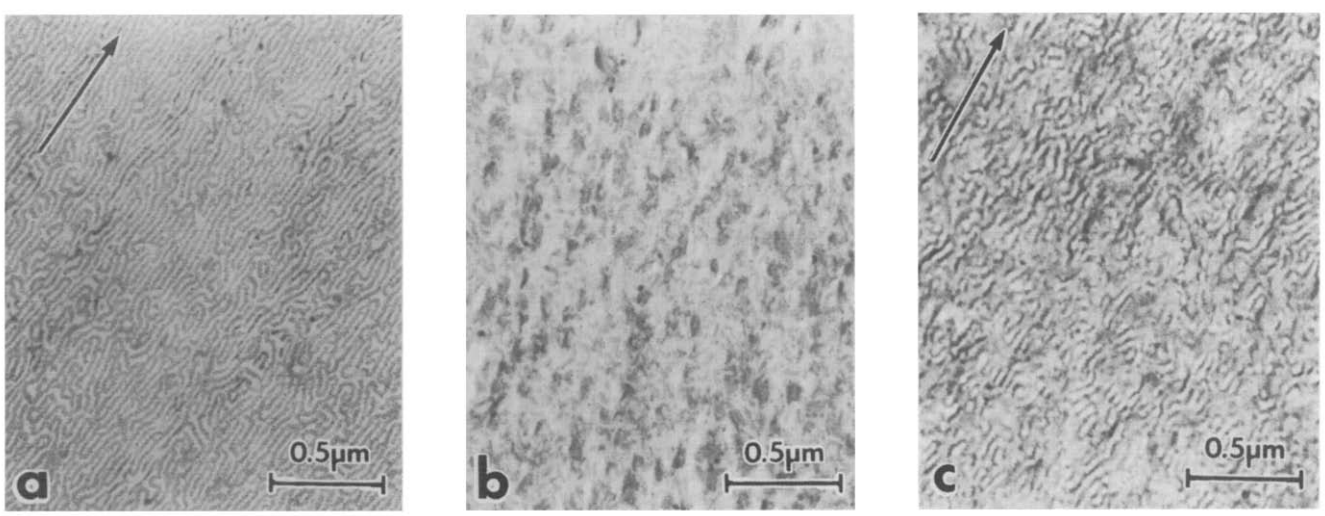

Figure 15 Transmission electron micrographs of injection-moulded KR05. The morphology was observed on the three different planes which meet at right angles as described in *Figure 2a*: (a) XY plane; (b) XZ plane; (c) YZ plane. The arrows show the injection directions

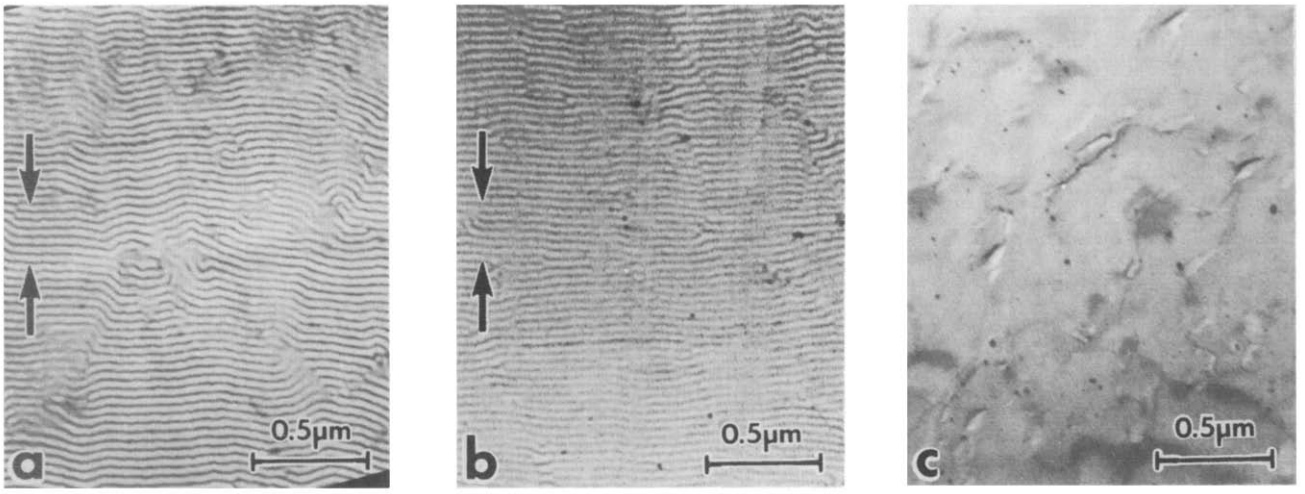

Figure 16 Transmission electron micrographs of 'slowly-cooled KR05'. The morphology was observed on the three different planes which meet at right angles as described in *Figure 2b*: (a) XY plane; (b) XZ plane; (c) YZ plane. The arrows show the compressive directions

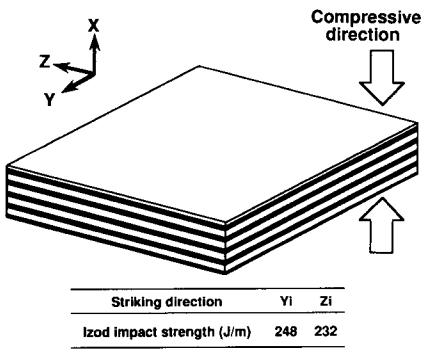

Figure 17 Speculative model of the stereoscopic microdomain structure of a 'slowly-cooled KR05' plaque. Note that the lamellar thickness is greatly exaggerated for the plaque dimensions. The table shows the notched Izod impact strength of test bars machined from the plaques. *Yi* and *Zi* show the pendulum-striking directions for impact test bars machined in the Z and Y directions, respectively

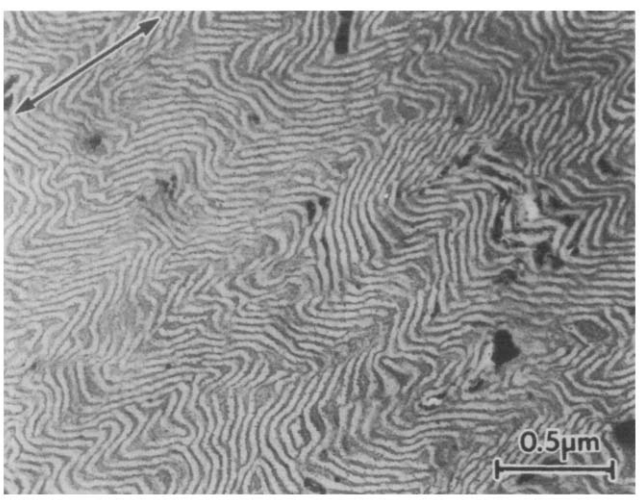

Figure 18 Transmission electron micrograph of 'slowly-cooled KR05' fractured under tensile stress. Morphological change was observed on a longitudinal cross-section just below the fracture surface. The arrow shows the tensile direction

mouldings (*Figures 4* and *15*) and for 'rapidly-cooled KR05' (*Figures 7* and *9*). This suggested that the stabilized interface and lamellar thicknesses of the melt hardly changed over a long cooling period.

Figure 17 represents a speculative model of the stereoscopic microdomain structure of 'slowly-cooled KR05' plaques at the inner regions where the end effects of the microdomain structure could be ignored. In this model, lamellar thickness is again greatly exaggerated for plaque size. The relaxation time of lattice disorder might be over the order of several minutes because very little lamellar disorder on the XY, XZ and YZ planes were seen for 'slowly-cooled KR05' plaques (*Figure 17*) in contrast to considerable lamellar disorder on the XY plane for 'rapidly-cooled KR05' (*Figure 10*). In 'slowly-cooled KR05' plaques, lamellae were oriented roughly parallel to plaque surfaces because of heat transfer normal to the surfaces on uniform cooling and, in addition, because of the sufficient relaxation of lamellar disorder in a long-sustained melt state.

The notched Izod impact strength of 'slowly-cooled KR05' plaques was not greatly varied with the MDs of the test bars (232 J m^{-1} in the Y direction and 248 J m^{-1} in the Z direction). This suggests that no mechanical anisotropy appeared in 'slowly-cooled KR05' plaques.

Figure 18 shows the deformation observed in the region close to the fracture surface after tensile stress application to the 'slowly-cooled KR05' specimen. The test bars of 'slowly-cooled KR05' were found to shear yield like those of 'rapidly-cooled KR05' machined in the Z direction (*Figure 8*). The lamellar orientation of 'slowly-cooled KR05' was roughly parallel to the direction in which stress was induced on mechanical testing as the test bars were machined in the Y or Z direction. Therefore, the fracture mechanism observed (*Figure 18*) seemed to differ from that proposed in a previous study[10], in which the styrene–butadiene block copolymer crazed rather than shear yielded when the lamellae were oriented in the stretching direction. The reason for this could be related to the slight lattice disorder and the consequent imperfect parallelism on the lamellae of 'slowly-cooled KR05' (*Figure 16*).

Since the test bars of 'slowly-cooled KR05' showed the same fracture mechanism as those of 'rapidly-cooled KR05' machined in the Z direction, it seemed natural that the former should have the same order of notched Izod impact strength as the latter ($\sim$240 J m^{-1} for the former and $\sim$230 J m^{-1} for the latter).

CONCLUSIONS

The mechanical properties of KR05 with lamellar type phase separation depend on the lamellar orientation. The KR05 mouldings of ordered lamellae are effectively toughened by shear yielding and incidental cavitation, and consequently show much higher notched Izod impact strength and larger elongation at break than those of wavy lamellae. In compensation for the excellent impact strength, the KR05 mouldings of ordered lamellae are inferior to those of wavy lamellae in rigidity and heat resistance. This is because the ordered lamellae of KR05 are subject to the large deformation of the PB soft phase in contrast to the large resistance against the deformation of the wavy lamellae of KR05 as the networks of the PB phase tangle with the PS rigid phase.

Stereoscopic structural examination of the KR05 mouldings revealed that the lamellae could be oriented normal to the direction of heat transfer and that the resultant stereoscopic anisotropy of the microdomain structure accounts for the appreciable mechanical anisotropy.

REFERENCES

1 Godovsky, Y. K. *Makromol. Chem., Suppl.* 1984, **6**, 117
2 Koltisko, B., Hiltner, A. and Baer, E. *J. Polym. Sci., Polym. Phys. Edn* 1986, **24**, 2167
3 Lewis, P. R. and Price, C. *Polymer* 1972, **13**, 20
4 Gohil, R. M. *Colloid Polym. Sci.* 1986, **264** (10), 847
5 Keller, A., Pedemonte, E. and Willmouth, F. M. *Kolloid Z.* 1970, **238**, 385
6 Argon, A. S., Cohen, R. E., Jang, B. Z. and Vander Sande, J. B. *J. Polym. Sci., Polym. Phys. Edn* 1981, **19**, 253
7 Schwier, C. E., Argon, A. S. and Cohen, R. E. *Phil. Mag. A* 1985, **52** (5), 581
8 Schwier, C. E., Argon, A. S. and Cohen, R. E. *Polymer* 1985, **26**, 1985
9 Wu, S. *Polymer* 1985, **26**, 1855
10 Ramsteiner, F. and Heckmann, W. *Polym. Commun.* 1984, **25**, 178
11 Bi, L.-K. and Fetters, L. J. *Macromolecules* 1976, **9**, 732
12 Hobbs, S. Y. *J. Macromol. Sci., Rev. Macromol. Chem.* 1980, **C19** (2), 221
13 Tadmor, Z. *J. Appl. Polym. Sci.* 1974, **18**, 1753
14 Hashimoto, T., Fujimura, M., Kawai, H., Diamont, J. and Shen, M. *Am. Chem. Soc., Div. Polym. Chem. Polym. Prepr.* 1978, **19** (1), 81
15 Fujimura, M., Hashimoto, T. and Kawai, H. *Rubber Chem. Technol.* 1978, **51** (2), 215
16 Hashimoto, H., Fujimura, M., Saijo, K. and Kawai, H. *Am. Chem. Soc. Adv. Chem. Ser.* 1979, **176**, 257
17 Phillips 66 Company. The K-Resin technical document for properties and processing, 1988
18 Hashimoto, T., Shibayama, M. and Kawai, H. *Macromolecules* 1980, **13**, 1237
19 Hashimoto, T., Nagatoshi, K., Todo, A., Hasegawa, H. and Kawai, H. *Macromolecules* 1974, **7**, 364
20 Inoue, T., Soen, T., Hashimoto, T. and Kawai, H. *J. Polym. Sci. A2* 1969, **7**, 1283
21 Leibler, L. *Macromolecules* 1980, **13**, 1602
22 Han, C. D., Kim, J. and Kim, J. K. *Macromolecules* 1989, **22**, 383
23 Cruz, M. O. and Sanchez, I. C. *Macromolecules* 1986, **19**, 2501
24 Hashimoto, T., Tsukahara, Y. and Kawai, H. *J. Polym. Sci., Polym. Lett. Edn* 1980, **18**, 585
25 'Polymer Alloys: Fundamentals and Applications', The Society of Polymer Science, 1st Edn, Tokyo Kagaku-dojin, Tokyo, 1981, p. 247
26 Chung, C. I. and Gale, J. C. *J. Polym. Sci., Polym. Phys. Edn* 1976, **14**, 1149
27 Chung, C. I. and Lin, M. I. *J. Polym. Sci., Polym. Phys. Edn* 1978, **16**, 545
28 Chung, C. I., Griesbach, H. L. and Young, L. *J. Polym. Sci., Polym. Phys. Edn* 1980, **18**, 1237
29 Gouinlock, E. V. and Porter, R. S. *Polym. Eng. Sci.* 1977, **17** (8), 535